sustainability

MDPI

Article

Improving Stress-Strain Behavior of Waste Aggregate Concrete Using Affordable Glass Fiber Reinforced Polymer (GFRP) Composites

Kittipoom Rodsin [1], Nazam Ali [2], Panuwat Joyklad [3,*], Krisada Chaiyasarn [4], Ahmed W. Al Zand [5,*] and Qudeer Hussain [6]

[1] Center of Excellence in Structural Dynamics and Urban Management, Department of Civil and Environmental Engineering Technology, College of Industrial Technology, King Mongkut's University of Technology North Bangkok, Bangkok 10800, Thailand; kittipoom.r@cit.kmutnb.ac.th
[2] Department of Civil Engineering, University of Management and Technology, Lahore 54770, Pakistan; nazam.ali@umt.edu.pk
[3] Department of Civil and Environmental Engineering, Faculty of Engineering, Srinakharinwirot University, Nakhonnayok 26120, Thailand
[4] Thammasat Research Unit in Infrastructure Inspection and Monitoring, Repair and Strengthening (IIMRS), Thammasat School of Engineering, Faculty of Engineering, Thammasat University Rangsit, Pathum Thani 12000, Thailand; ckrisada@engr.tu.ac.th
[5] Department of Civil Engineering, Faculty of Engineering and Built Environment, Universiti Kebangsaan Malaysia (UKM), Bangi 43600, Selangor, Malaysia
[6] Center of Excellence in Earthquake Engineering and Vibration, Department of Civil Engineering, Chulalongkorn University, Bangkok 10330, Thailand; ebbadat@hotmail.com
* Correspondence: panuwatj@g.swu.ac.th (P.J.); ahmedzand@ukm.edu.my (A.W.A.Z.)

Citation: Rodsin, K.; Ali, N.; Joyklad, P.; Chaiyasarn, K.; Al Zand, A.W.; Hussain, Q. Improving Stress-Strain Behavior of Waste Aggregate Concrete Using Affordable Glass Fiber Reinforced Polymer (GFRP) Composites. *Sustainability* **2022**, *14*, 6611. https://doi.org/10.3390/su14116611

Academic Editor: Yuan Chen

Received: 5 May 2022
Accepted: 26 May 2022
Published: 28 May 2022

Abstract: Several studies have highlighted the potential of crushed brick aggregates in non-structural concrete. This is because crushed brick aggregates offer substandard mechanical properties in comparison to natural stone aggregates. Synthetic Fiber Reinforced Polymer (FRP) sheets have been known to overcome this issue. However, enormous costs associated with synthetic FRPs may limit their use in several low-budget applications. This study recognizes this issue and propose a cost-effective solution in the form of low-cost glass fiber (LC-GFRP) sheets. Two types of brick aggregates (i.e., solid-clay and hollow-clay brick aggregates) were used to fabricate concrete by replacing 50% of natural aggregates. Experimental results of 32 non-circular specimens were reported in this study. To overcome the substandard mechanical properties of recycled brick aggregate concrete (RBAC), specimens were strengthened with 2, 4, and 6 layers of LC-GFRP sheets. Noticeable improvements in ultimate compressive stress and corresponding strain were observed and were found to correlate positively with the number of LC-GFRP sheets. It was found that 4 and 6 layers of LC-GFRP sheets imparted significant axial ductility irrespective of the brick aggregate type and inherent concrete strength. Several existing stress-strain models for confined concrete were considered to predict ultimate confined compressive stress and corresponding strain. Accuracy of existing models was assessed by mean of the ratio of analytical to experimental values and associated standard deviations. For ultimate stress predictions, the lowest mean value of the ratio of analytical to experimental ultimate compressive stress was 1.07 with a standard deviation of 0.10. However, none of the considered models was able to provide good estimates of ultimate strains.

Keywords: low-cost confinement; LC-GFRP; ultimate compressive stress; ultimate compressive stress-strain models; non-circular specimens

1. Introduction

In recent years, demolition of existing buildings has caused massive accumulation of waste around the world. China alone produces 1.8 billion tons of waste from demolition of existing buildings [1]. Two problems are emphasized in this regard. On one hand, proper disposal of such gigantic number of wastes is hideous, whereas scarcity of raw aggregates has been developing [2]. A possible solution lies in the reuse of this generated waste. This not only prevents the accumulation of massive wastes, but it also reduces the readily increasing scarcity of raw aggregates. Further, the costs associated with proper disposal of construction waste could also be reduced. Thus, the need for a sustainable, cost-effective, and a green environment friendly solution is emphasized. Therefore, several existing studies have highlighted the potential of recycled aggregate concrete (RAC) to construct reinforced concrete structures [3–7].

As per The International Union of Laboratories and Experts in Construction Materials Systems and Structures (RILEM), recycled aggregates are classified into three groups generated from (1) demolished masonry structures (2) wastes of concrete structures and (3) mixture of both natural and recycled aggregates [8]. Clay bricks are one of the most readily available construction elements around the globe. Their low-cost and easy application have eased their way into construction industry noticeably. Consequently, construction and demolition waste (CDW) generated each year comprises a noticeable amount of clay brick waste. It has been stated that approximately 1 billion tons of CDW is produced in European Union each year with bricks as a key component [9]. Therefore, recycled clay brick aggregates (CBA) are prevalently used in the production of RAC to reduce their detrimental effects on environment [10]. The potential of RAC constructed with CBA (RBAC) has been investigated in the construction of structural elements [11–16]. Several advantages and disadvantages of RBAC have been highlighted compared with normal coarse aggregate concrete (NAC). Main advantages of RBAC arise from its relatively light weight due to their lower density as compared to that of NAC [16,17]. Further, RBAC offers better resistance to fire that can be ascribed to the excellent intrinsic refractory characteristics of clay bricks [15]. On the other hand, it has been reported that RBAC exhibits inferior mechanical properties [18–20]. Further, RBAC exhibits lower resistance to carbonization and chloride attacks [21] and high porosity [16,17,22]. These substandard characteristics of RBAC have limited its use to non-structural applications [23].

To enhance these substandard mechanical properties of RBAC (i.e., their ultimate compressive strength and the corresponding strain), a viable solution has been practiced by wrapping RBAC with fiber reinforced polymer jackets. Gao et al. [24] strengthened RBAC with glass and carbon fiber reinforced polymer (FRP) jackets. It was found that the ultimate compressive strength decreased as the replacement ratio of brick aggregates increased. However, the application of glass and carbon FRP wraps enhanced ultimate strength and corresponding strain of RBAC. Several other studies have also highlighted similar enhancements in the mechanical behavior of RBAC from external synthetic FRP wraps [25–28]. Although synthetic FRP confinement has proved to impart significant gains in ultimate compressive strength and corresponding strain, their high costs are a serious concern from overall rehabilitation cost analysis [10,29,30]. Therefore, this study explores strength and ductility enhancement of RBAC arising from external wraps of low-cost glass FRP composites. Yoddumrong et al. [31] utilized low-cost glass fiber reinforced polymer composite jackets (LC-GFRP) to strengthen RC columns. Commercially available LC-GFRP jackets were used for this purpose that comprised bi-directional glass fiber sheets. Their salient features included extremely low cost but adequate tensile strength. Rodsin et al. [32] extended the use of LC-GFRP jackets to strengthen very low (i.e., 5 and 15 MPa) strength concrete. It was concluded that LC-GFRP successfully enhanced ultimate strength and ductility of concrete.

The aforesaid discussion emphasizes the need for the reuse of brick waste to reduce its detrimental environmental impacts. Despite of several studies highlighting the potential of recycled brick aggregates to replace normal coarse aggregates in concrete, substandard mechanical properties of the resulting concrete must be dealt with caution. Though synthetic FRPs have been known to overcome this issue, their massive costs may limit their application. An alternative solution is recognized in the use of low-cost GFRP jackets.

To authors knowledge, no experimental study is conducted till date to investigate the performance of this type of jackets on recycled brick aggregate concrete.

This study intends to extend the application of LC-GFRP in the strengthening of RBAC. Therefore, the following objectives are recognized (1) to strengthen RBAC to potentially qualify in structural applications and (2) to achieve this objective using LC-GFRP. These objectives were chosen to provide a sustainable and environment friendly solution for the waste generated from demolition of existing brick masonry. Further, a cost-effective solution was potentially found in the use LC-GFRP rather than employing expensive synthetic FRP sheets.

2. Experimental Program

2.1. Test Matrix

This study comprised an experimental program on 32 concrete rectilinear concrete specimens with and without external LC-GFRP strengthening. Each specimen measured $150 \times 150 \times 300$ $(width \times depth \times height\ in\ \text{“}mm\text{”})$. In this study, all square specimens were cast with a cross-section and height of 150 × 150 mm and 300 mm respectively, to achieve height to cross-sectional width ratio of 2.0. The size effect is an important factor affecting the confinement effectiveness of the column. In previous studies, the effectiveness of CFRP wraps to enhance ultimate strength is found higher for short columns than slender columns. However, the size effect was not considered in this study. Specimens were categorized in two main groups depending upon the constituting brick aggregate types. Specimens in each group were further subdivided in two subgroups depending upon the concrete strength. Therefore, each subgroup comprised 8 specimens. Out of those 8 specimens, two specimens were tested in as-built condition and served as reference for that subgroup. Two specimens each were strengthened with 2, 4, and 6 layers of LC-GFRP. A three-part nomenclature was adopted in this study. First part referred to the concrete strength i.e., LS and HS for low and high strength concrete, respectively. Second part referred to the constituting brick aggregates i.e., CBA and CBB for crushed brick aggregates originating from type A and B bricks, respectively. Last part denoted the presence/amount of external LC-GFRP sheets. For control specimen, abbreviation of “CON” was used whereas 2L, 4L, and 6L were used for 2, 4, and 6 layers of LC-GFRP sheets, respectively. Further details are presented in Table 1. 50% of natural aggregates in both concretes were replaced with recycled crushed brick aggregates.

Table 1. Test matrix.

Specimens	Concrete Strength	Brick Type	GFRP Layers	Number of Specimens
LS-CBA-CON	LS	Type A	-	2
LS-CBA-2L	LS	Type A	2	2
LS-CBA-4L	LS	Type A	4	2
LS-CBA-6L	LS	Type A	6	2
HS-CBA-CON	HS	Type A	-	2
HS-CBA-2L	HS	Type A	2	2
HS-CBA-4L	HS	Type A	4	2
HS-CBA-6L	HS	Type A	6	2
LS-CBB-CON	LS	Type B	-	2
LS-CBB-2L	LS	Type B	2	2
LS-CBB-4L	LS	Type B	4	2
LS-CBB-6L	LS	Type B	6	2
HS-CBB-CON	HS	Type B	-	2
HS-CBB-2L	HS	Type B	2	2
HS-CBB-4L	HS	Type B	4	2
HS-CBB-6L	HS	Type B	6	2

2.2. Material Properties

Two types of concrete were used in this study to examine the effect of concrete strength on the confinement efficiency of LC-GFRP sheets. Concrete was categorized as low and high strength corresponding to the target ultimate compressive strength values of 15 and 35 MPa, respectively. Both types of concretes utilized type-I Portland cement. Maximum size of natural and crushed brick aggregates was limited to 25 mm. Table 2 provides mix ratios for the two concrete batches. Required amount of water was determined to target slump value of 90 and 70 mm for low and high strength concrete, respectively.

Table 2. Mix ratios for two concrete types.

Mix Ingredients (kg/m^3)	Low Strength Concrete (15 MPa)	High Strength Concrete (35 MPa)
Cement	242	444
Fine aggregates	726	605
Natural coarse aggregates	605	504
Clay brick aggregates	605	504

Fired-clay solid and hollow bricks were used to replace 50% of natural aggregates in each concrete batch. Figure 1 shows the types of bricks used in this study. Mechanical properties of bricks (Table 3) were determined in accordance with ASTM standards [33,34]. River sand was used as fine aggregate.

(**a**)

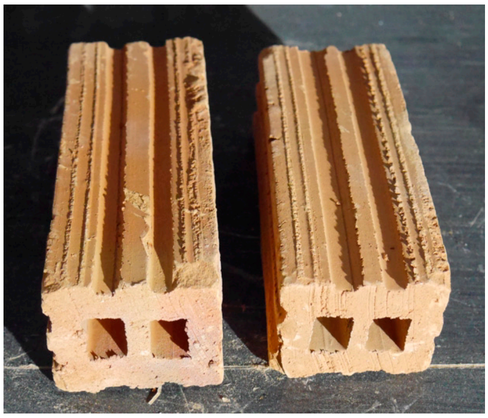

(**b**)

Figure 1. Bricks used (**a**) clay solid and (**b**) clay hollow.

Table 3. Mechanical properties of bricks.

Type of Bricks	Density of Bricks (kg/m^3)	Compressive Strength of Bricks (MPa)	Water Absorption of Bricks (%)
Type A	120	3.14	23.27
Type B	140	8.10	16.58

Low-cost GFRP sheets were fabricated from locally available bidirectional glass fibers (see Figure 2a) and polyester resin. Standard tensile coupons of LC-GFRP were used to determine their mechanical properties. Figure 2b shows typical failure of LC-GFRP sheets. Further, these coupons were prepared from 1, 2, 3, 4, and 5 layers of LC-GFRP sheets to investigate thickness effect on mechanical properties. For each thickness type, three coupons were tested. This adopted procedure followed the recommendations of ASTM D3013-13 [35]. Mechanical properties of LC-GFRP sheets and epoxy resin are summarized in Table 4.

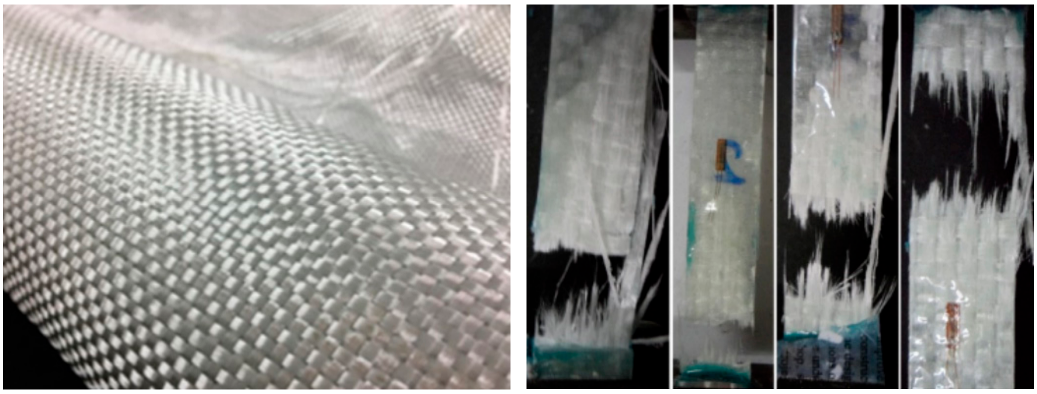

(**a**) (**b**)

Figure 2. (**a**) Bidirectional GFRP sheet and (**b**) typical tensile failure of LC-GFRP.

Table 4. Mechanical properties of strengthening system.

Composite	Tensile Stress (MPa)	Ultimate Strain (%)	Elastic Modulus (GPa)	Standard Deviation
Epoxy	17.20	0.632	2.72	1.09
LC-GFRP	377.64	2.040	18.70	1.91

2.3. Preparation of Test Specimens

Concrete was cast using standard steel molds in laboratory environment. Molds were removed after 1 day of the concrete casting. Following that, specimens were cured for a period of 28 days in ambient conditions. It has been known that confinement effectiveness of external sheets is reduced in rectilinear sections due to the stress concentrations near corners [36,37]. Therefore, corners of rectilinear sections were rounded off to a corner radius of 13 mm. On 28th day, external LC-GFRP system was applied as per the recommendations of ACI code [38]. Concrete surface was thoroughly cleaned. In the first step, resin was applied onto the concrete surface using a hand brush. Then, resin impregnated GFRP sheets were carefully applied to the concrete surface. Proper care was taken to eliminate the presence of any voids. A similar procedure was repeated for the application of additional GFRP layers. Figure 3 presents the application of GFRP sheets on concrete specimens.

(**a**) (**b**) (**c**)

Figure 3. (**a**) Application of GFRP sheet (**b**) application of resin and (**c**) strengthened specimens.

2.4. Instrumentation & Test Setup

A detailed setup was planned to measure applied axial load and corresponding axial deformation of concrete specimens. A Universal Testing Machine was used to apply monotonically increasing axial load. Smoothening of the top and bottom surfaces of specimens was performed to ensure uniform application of the load. Load concentration was assured by placing steel plates below and above the bottom and top surfaces, respectively. Axial deformation of each specimen was recorded using two Linear Variable Differential Transducers (LVDTs). The pre-calibrated LVDTs were vertically mounted on a steel plate and pointed with the loading plate of UTM at the top of the concrete specimens as shown in Figure 4.

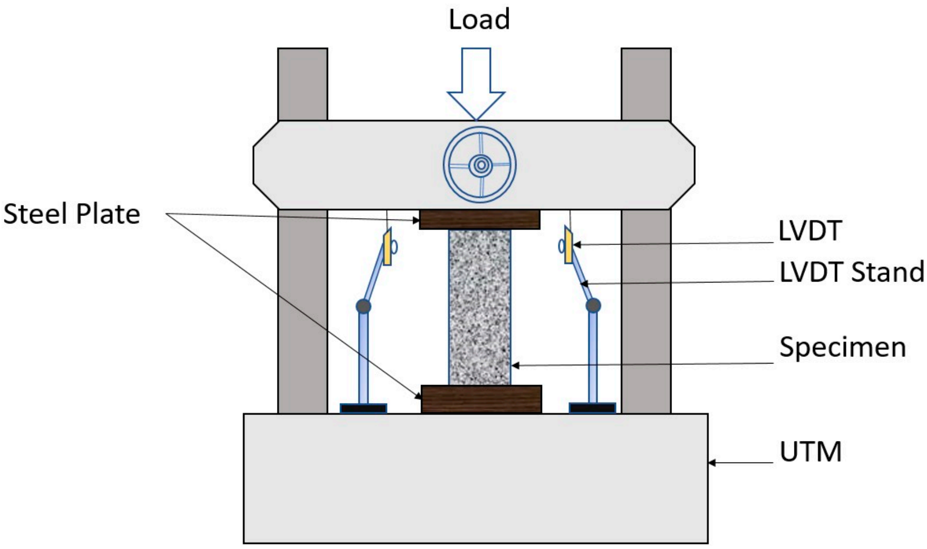

Figure 4. Schematics of test setup.

3. Experimental Results

3.1. Ultimate Failure Modes

Figure 5 presents ultimate failure modes of all specimens. These failure modes are representative of the two specimens for each specimen type. Failure mode of the control specimens accompanied excessive concrete crushing and splitting along the full height. In general, a delay and extent of crushing was observed in LC-GFRP confined specimens. For LC-GFRP confined specimens, failure was initiated by the rupture of GFRP sheets along the height of specimens. It is to be mentioned that the failure of LC-GFRP did not occur at corners except of those strengthened with 6 layers of LC-GFRP. It emphasizes that a provision of 13 mm corner radius was sufficient to shift failure of LC-GFRP from corners to the sides ensuring a more uniform distribution of confinement pressure across the section. A similar result was also highlighted by Hussain et al. [39]. Further, all strengthened specimens demonstrated severe damage and excessive dilation of their sides. For specimens confined with 6 layers of LC-GFRP, highest axial loads and corresponding strains were observed. As a result, they experienced highest lateral dilations due to Poisson's effect. As stated, rupture of LC-GFRP was observed near corners for some of the specimens. It has been reported that the effectiveness of external confinement correlates positively with the magnitude of corner radius [40]. Therefore, a larger than 13 mm corner radius would have further improved the stress distributions as well as the confinement effectiveness of external LC-GFRP sheets across the section. Nonetheless, application of LC-GFRP in combination with a 13 mm corner radius significantly delayed the failure of specimens. This delay was observed in all strengthened specimens irrespective of the number of external LC-GFRP layers.

Figure 5. Ultimate failure modes.

3.2. Axial Load-Deflection Curves

Figure 6 presents experimental axial load-deformation response of all specimens. In Figure 6a, it is evident that the control specimen LS-CBA-CON experienced lowest ultimate stress and the corresponding strain. It could only sustain ultimate stress of 8.40 MPa whereas ultimate recorded strain was 0.008. Specimen strengthened with two layers of LC-GFRP (i.e., LS-CBA-2L) exhibited a 53 and 31% increase in ultimate stress and strain, respectively. In the case of four layers, a 131 and 214% increase in ultimate stress and strain, respectively was observed. Whereas a 237 and 360% increase in ultimate stress and strain was observed for the case of 6 layers i.e., in specimen LS-CBA-6L. Further, a ductile post-peak stress-strain response was observed for the case of 4- and 6-layer LC-GFRP confinement. Figure 6b presents stress-strain curves of subgroup HS-CBA. Control specimen HS-CBA-CON was able to withstand ultimate stress of 18.2 MPa at an ultimate strain of 0.0079. Application of 2, 4, and 6 layers of LC-GFRP increased the ultimate stress by 15, 49, and 88%, respectively. Same configuration of LC-GFRP improved ultimate strain by 15, 207, and 301%, respectively. Analogous to subgroup LS-CBA, specimens confined with 4 and 6 LC-GFRP layers exhibited a bilinear stress-strain response and ultimate stress was sustained for large strain values. Whereas a sudden drop in ultimate stress was observed for the case of 2-layer LC-GFRP confinement.

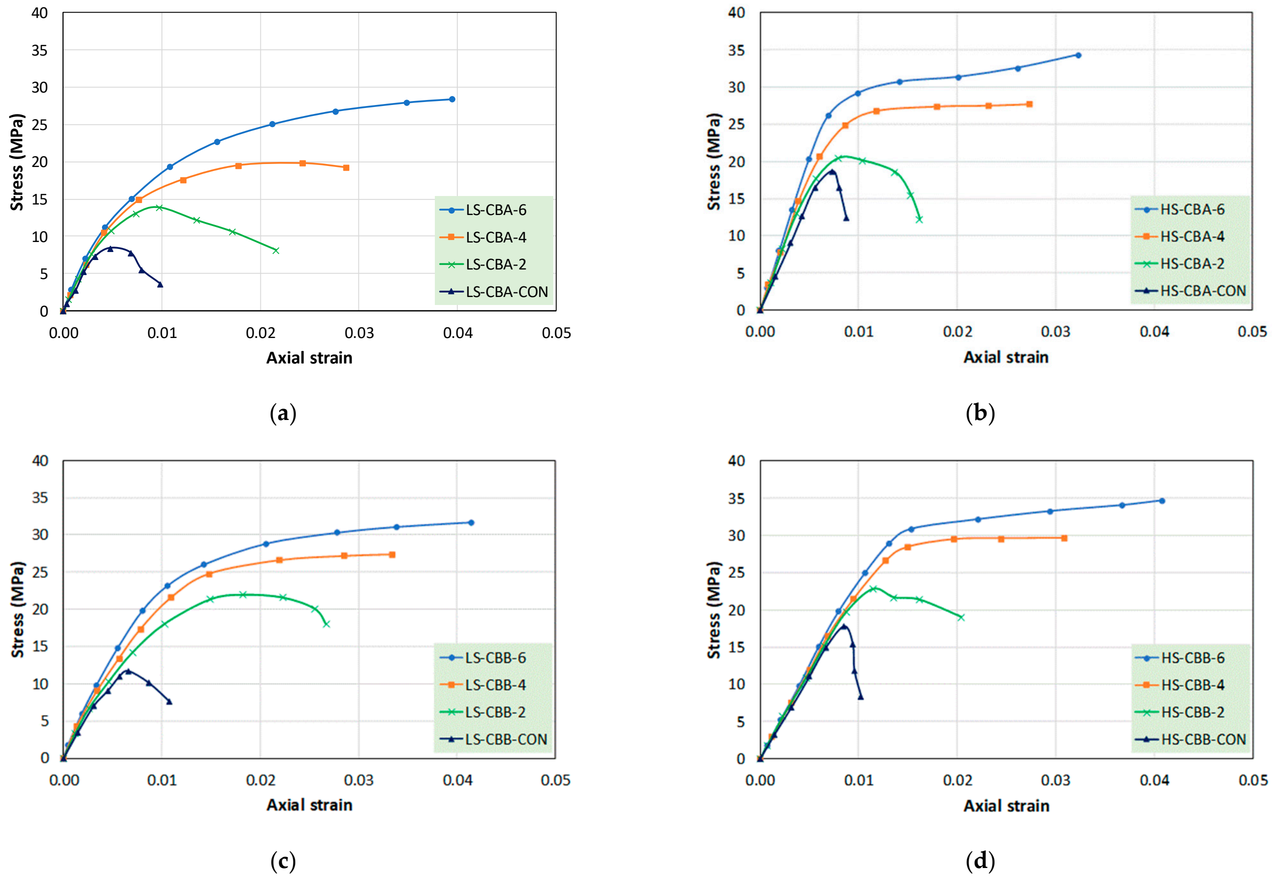

Figure 6. Ultimate stress versus strain response for subgroup (**a**) LS-CBA (**b**) HS-CBA (**c**) LS-CBB and (**d**) HS-CBB.

Figure 6c shows axial stress-strain response of subgroup LS-CBB. Ultimate stress and strain sustained by the control specimen were 11.1 MPa and 0.0063, respectively. Application of 2, 4, and 6 layers of LC-GFRP increased the ultimate stress by 92, 138, and 186%, respectively. Similar configurations of LC-GFRP increased the ultimate strain by 167, 359, and 553%, respectively. Again, 4 and 6 layers of LC-GFRP were able to impart sufficient axial ductility in contrast of the control and 2-layer LC-GFRP confined specimens. Finally, axial stress and strain response of the subgroup HS-CBB is shown in Figure 6d. Again, ultimate stress and strain exhibited a positive correlation with the number of external LC-GFRP layers and 4 and 6 layers of LC-GFRP were found to impart significant axial ductility to the axial response of corresponding specimens. Table 5 summarizes detailed results of all four subgroups.

Table 5. Summary of experimental results.

Specimens	Ultimate Stress (MPa)	Increase in Ultimate Stress (%)	Ultimate Strain	Increase in Ultimate Strain (%)
LS-CBA-CON	8.40	-	0.0080	-
LS-CBA-2L	12.9	53	0.0104	31
LS-CBA-4L	19.5	131	0.0251	214
LS-CBA-6L	28.3	237	0.0368	360
HS-CBA-CON	18.2	-	0.0079	-
HS-CBA-2L	20.9	15	0.0091	15
HS-CBA-4L	27.1	49	0.0242	207
HS-CBA-6L	34.2	88	0.0317	301
LS-CBB-CON	11.1	-	0.0063	-
LS-CBB-2L	21.3	92	0.0169	167
LS-CBB-4L	26.4	138	0.0291	359
LS-CBB-6L	31.8	186	0.0414	553
HS-CBB-CON	18.2	-	0.0070	-
HS-CBB-2L	23.6	30	0.0135	93
HS-CBB-4L	29.9	64	0.0248	254
HS-CBB-6L	34.8	91	0.0333	375

Note: “-” refers to the control specimens (where increase in either ultimate stress or strain is not applicable).

3.3. Effect of LS-GFRP Layers & Concrete Strength

The effect of concrete strength on the improvements imparted by LC-GFRP sheets in the ultimate stress and corresponding strain is graphically shown in Figure 7. For clarity, improvements in ultimate stress and the corresponding strain for low and high strength concrete specimens are shown by red and blue markers, respectively. A common trend can be observed in Figure 7a–d. For similar configurations of LC-GFRP confinement, improvements imparted to ultimate stress and the corresponding strain of low strength concrete specimens were consistently higher than those of high strength concrete specimens. Apart from Figure 7b, this trend can be found prevalent. This suggests that the efficiency of LC-GFRP in terms of axial stress and corresponding strain enhancement is dependent on and inversely related to the inherent concrete strength. Effect of the number of LC-GFRP layers on the improvement in ultimate stress and corresponding strain can also be studied from Figure 7. A linear trend in the increase in ultimate stress and corresponding strain was observed as the number of external LC-GFRP layers increased.

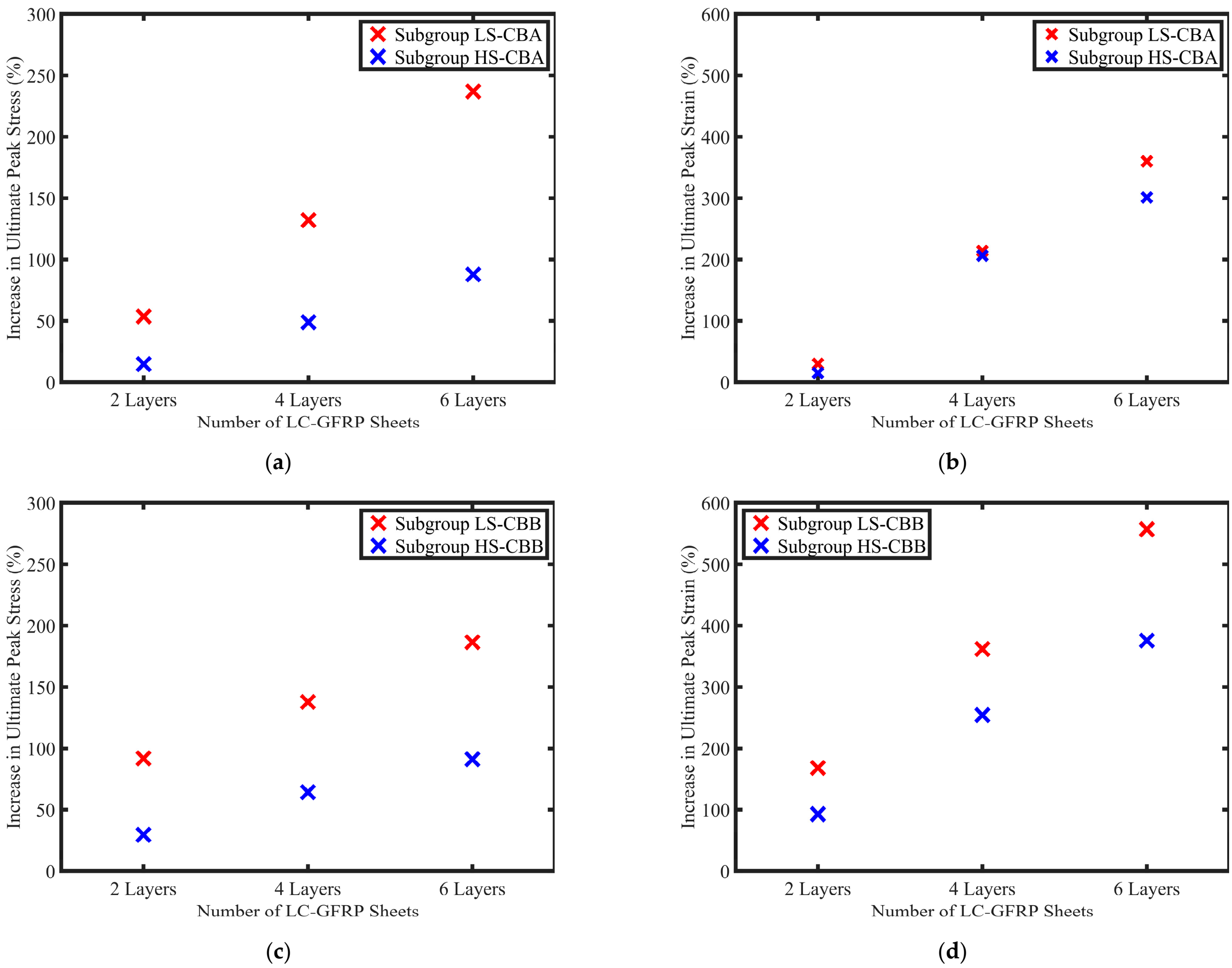

Figure 7. Effect of concrete strength and number of LC-GFRP layers on (**a**) Ultimate stress of group 1 (**b**) ultimate strain of group 1 (**c**) ultimate stress of group 2 and (**d**) ultimate strain of group 2 specimens.

3.4. Effect of Type of Bricks

This study replaced 50% of natural aggregates in both concrete types by crushed brick aggregates. For group 1, brick aggregates were obtained from hollow-clay brick aggregates whereas solid-clay bricks were crushed to obtain aggregates for group 2 specimens. Figure 8 presents comparison of increase in ultimate stress and corresponding strain for the two types of bricks. For clarity, top figures are plotted for low strength concrete whereas bottom figures are plotted for high strength concrete specimens. For low strength specimens, it is evident that the improvement in both ultimate stress and corresponding strain was higher for solid-clay brick aggregate specimens than those with hollow-clay brick aggregates. An exception was observed for the case of 6-layer LC-GFRP confined specimen where the increase in ultimate stress was observed higher for hollow-brick specimens. However, this peculiar observation can be considered an outlier and therefore attributed to the unforeseen measurement errors. Analogous to low strength concrete specimens, improvement in ultimate stress and corresponding strain was consistently higher for solid-brick aggregate specimen than that of the hollow-brick aggregate specimens. This suggests that for similar concrete strength and external LC-GFRP configuration, specimens fabricated with hollow brick aggregates as partial replacement of normal coarse aggregates may perform inferior to those fabricated with solid-brick aggregates.

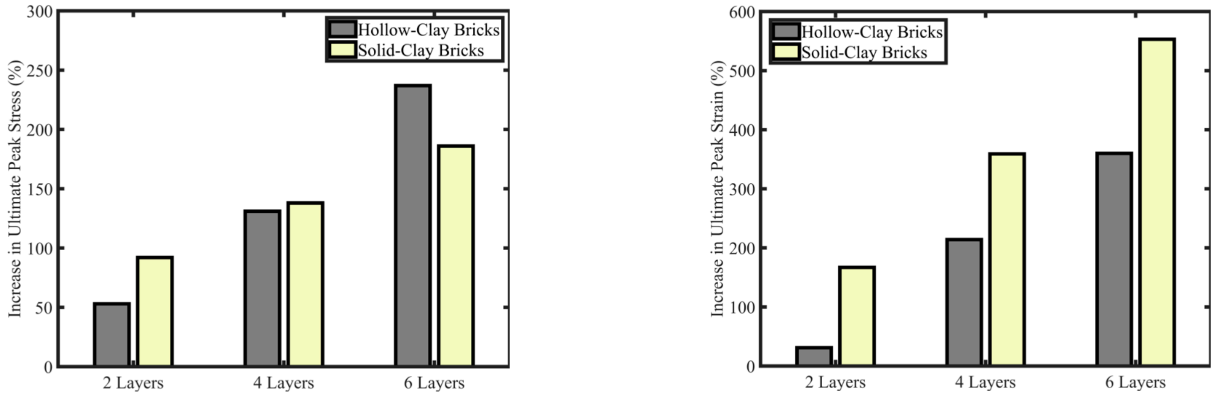

Low concrete strength specimens (**left**) peak stress and (**right**) peak strain

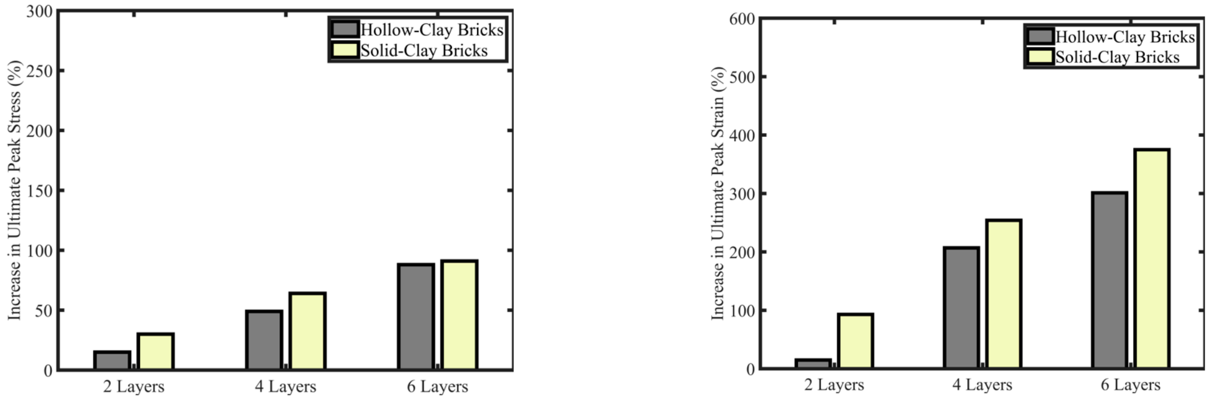

High concrete strength specimens (**left**) peak stress and (**right**) peak strain

Figure 8. Comparison of gain in peak stress and corresponding strain as a function of brick aggregate type.

4. Analytical Investigations

4.1. Compressive Strength Models

Different equations have been proposed till date to express axial strength enhancement in terms of externally applied FRPs [41,42]. The confined peak strength can be expressed in the following form:

$$\frac{f_{cc}}{f'_c} = 1 + k_1 \frac{f_l}{f'_{co}} \tag{1}$$

where f_{cc} represents peak compressive strength due to LC-GFRP confinement, k_1 represents coefficient of external confinement. f_l is the lateral passive confining pressure generated from external GFRP sheets and it is expressed in the following form by considering the equilibrium between the pressure from outward expansion and the resulting external confining pressure as shown in Figure 9 and given in Equation (2).

$$f_l = \frac{2 f_t t}{D} \times \rho \tag{2}$$

where D represents the diagonal length of non-circular sections and f_t is the tensile strength of LC-GFRP. The diagonal length D can be calculated as [39].

$$D = \frac{2bd}{b + d} \tag{3}$$

where d and b are depth and width of section, respectively. ρ in Equation (2) can be determined from Equation (4) as per ACI-440.2 R-02 [38].

$$\rho = 1 - \frac{(b - 2R_c)^2 + (d - 2R_c)^2}{3A} \tag{4}$$

where R_c is corner radius and A is given in Equation (5).

$$A = bd - (4 - \pi)R_c^2 \tag{5}$$

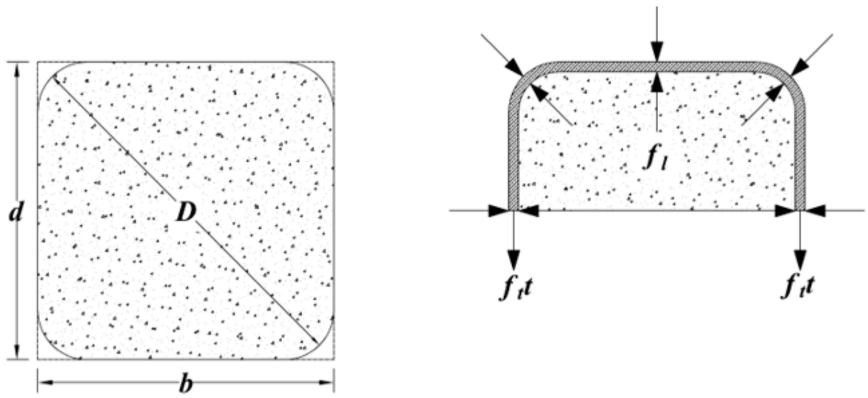

Figure 9. Confinement mechanism from external LC-GFRP.

4.2. Ultimate Strain Models

One of the earliest studies on lateral confining of concrete was performed by Richart et al. [43]. Ultimate strain in confined form can be related to externally applied pressure f_l from Equation (6).

$$\frac{\epsilon_{cc}}{\epsilon_{co}} = 1 + k_2 \frac{f_l}{f'_{co}} \tag{6}$$

where ϵ_{co} is the axial ultimate strain of unconfined concrete. Richart et al. [43] proposed a value of $5k_1$ for k_2 in the case of steel confined concrete. Later, several studies indicated that similar form of equation can be used for FRP confined concrete [41,44–46]. Table 6 presents several ultimate stress and strain models for externally confined non-circular sections.

Table 6. Summary of existing ultimate stress-strain models.

ID	Model	Ultimate Stress	Ultimate Strain
1	Shehata et al. [41]	$\frac{f_{cc}}{f'_{co}} = 1 + 0.85\left(\frac{f_l}{f'_{co}}\right)$	$\frac{\epsilon_{cc}}{\epsilon_{co}} = 1 + 13.5\left(\frac{f_l}{f'_{co}}\right)$
2	ACI 2002 [38]	$\frac{f_{cc}}{f'_{co}} = -1.254 + 2.254\sqrt{1 + \frac{7.94 f_l}{f'_{co}}} - 2\frac{f_l}{f'_{co}}$	$\frac{\epsilon_{cc}}{\epsilon_{co}} = 1.5 + 13\left(\frac{f_l}{f'_{co}}\right)\left(\frac{\epsilon_{fe}}{\epsilon_{co}}\right)^{0.45}$
3	Touhari and Mitiche [47]	$\frac{f_{cc}}{f'_{co}} = 1 + \left(1 - \frac{\left(\left(\frac{\pi}{2}\right)-1\right)(b-2R_c)^2}{b^2}\right)\frac{f_l}{f'_{co}}$	$\frac{\epsilon_{cc}}{\epsilon_{co}} = 2.3 + 7\left(1 - \frac{\left(\left(\frac{\pi}{2}\right)-1\right)(b-2R_c)^2}{b^2}\right)\frac{f_l}{f'_{co}}$
4	Hussain et al. [39]	$\frac{f_{cc}}{f'_{co}} = 1 + 2.70\rho^{0.90}\left(\frac{f_l}{f'_{co}}\right)$	$\frac{\epsilon_{cc}}{\epsilon_{co}} = 2 + 10\rho^{1.10}\left(\frac{f_l}{f'_{co}}\right)$
5	Mirmiran et al. [48]	$\frac{f_{cc}}{f'_{co}} = 1 + 6.0\left(\frac{2R_c}{D}\right)\left(\frac{f_l^{0.7}}{f'_{co}}\right)$	-
7	Lam and Teng [49]	$\frac{f_{cc}}{f'_{co}} = 1 + 3.30\left(\frac{f_l}{f'_{co}}\right)$	$\frac{\epsilon_{cc}}{\epsilon_{co}} = 1.75 + 12\left(\frac{f_l}{f'_{co}}\right)\left(\frac{\epsilon_{fe}}{\epsilon_{co}}\right)^{0.45}$

4.3. Assessment of Existing Stress-Strain Models

Figure 10 presents the comparison of experimental and analytical confined ultimate strengths of all subgroups. For subgroup LS-CBA, the model of Hussain et al. [39] provided closest proximity to the 45° line. The models of Mirmiran et al. [48], Shehata et al. [41], and

Touhari and Mitiche [47] underestimated the experimental values. Whereas the models of ACI 2002 [38] and Lam & Teng [49] overestimated experimental results. For subgroup HS-CBA, the models of ACI 2002 [38] and Lam & Teng [49] yielded higher values than experimental results of confined peak strengths. Whereas the models of, Shehata et al. [41], Touhari and Mitiche [47], and Mirmiran et al. [48] underestimated the experimental results. For subgroup LS-CBB in Figure 10c, it is apparent that the models of ACI 2002 [38] and Lam & Teng [49] seem to provide close approximates of experimental results whereas the models of Mirmiran et al. [48], Shehata et al., Hussain et al. [39], and Touhari and Mitiche [47] formed the lower bounds. For subgroup HS-CBB, apart from the model of Hussain et al. [39], none of the considered models provided good agreement with experimental results.

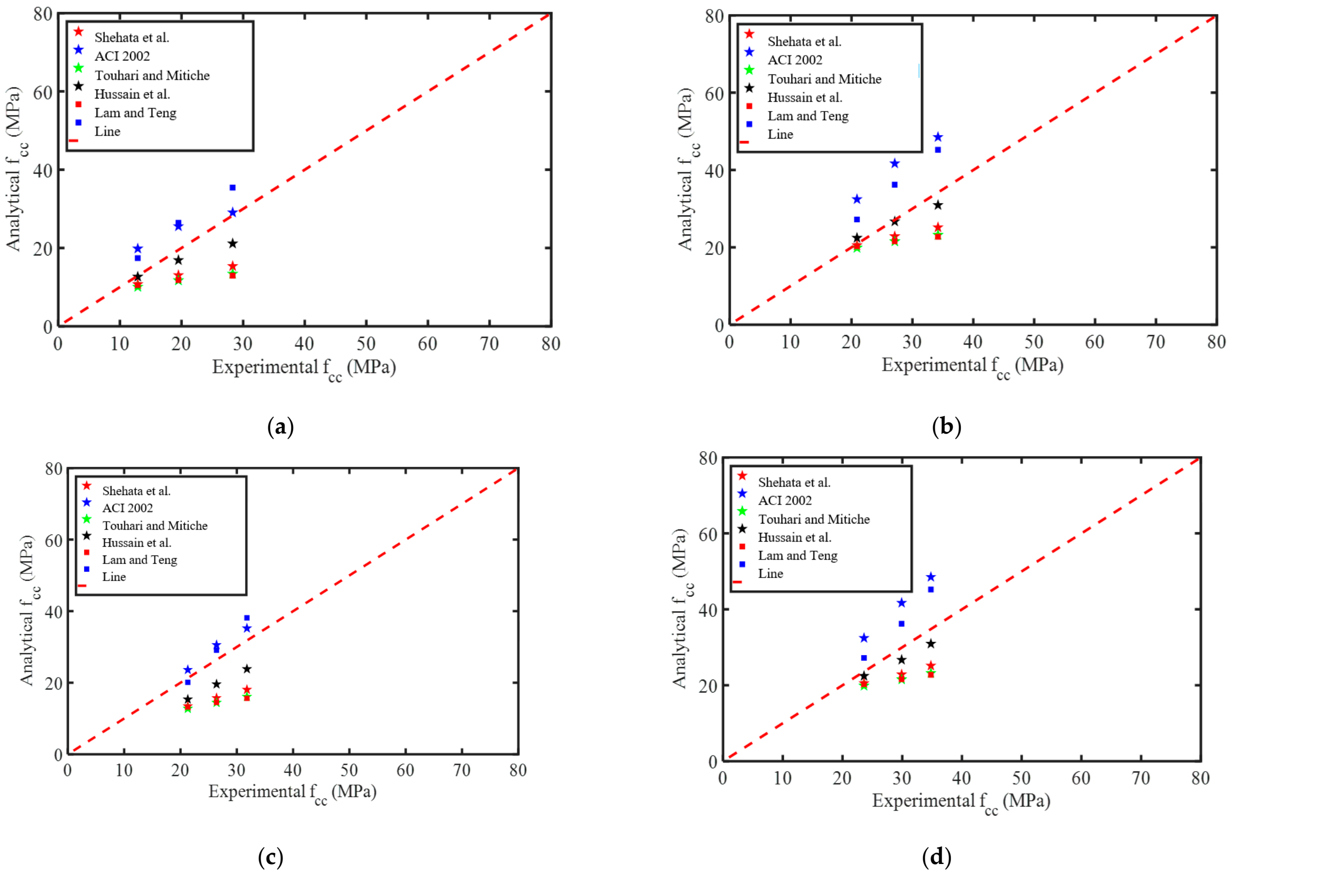

Figure 10. Comparison of experimental and analytical confined f_{cc} for subgroup (**a**) LS-CBA (**b**) HS-CBA (**c**) LS-CBB and (**d**) HS-CBB.

Figure 11 presents comparison of experimental and analytical peak compressive strains. It is evident from Figure 11a that all the models overestimated peak compressive strains of specimens in subgroup LS-CBA. The scatter was reduced for subgroup HS-CBA (Figure 11b) with the models of Hussain et al. [39] and Touhari and Mitiche [47] providing closest agreement with experimental values. For subgroups LS-CBB and HS-CBB, the models of Hussain et al. [39] and Touhari and Mitiche [47] again provided closest match with experimental values whereas all other models overestimated experimental values.

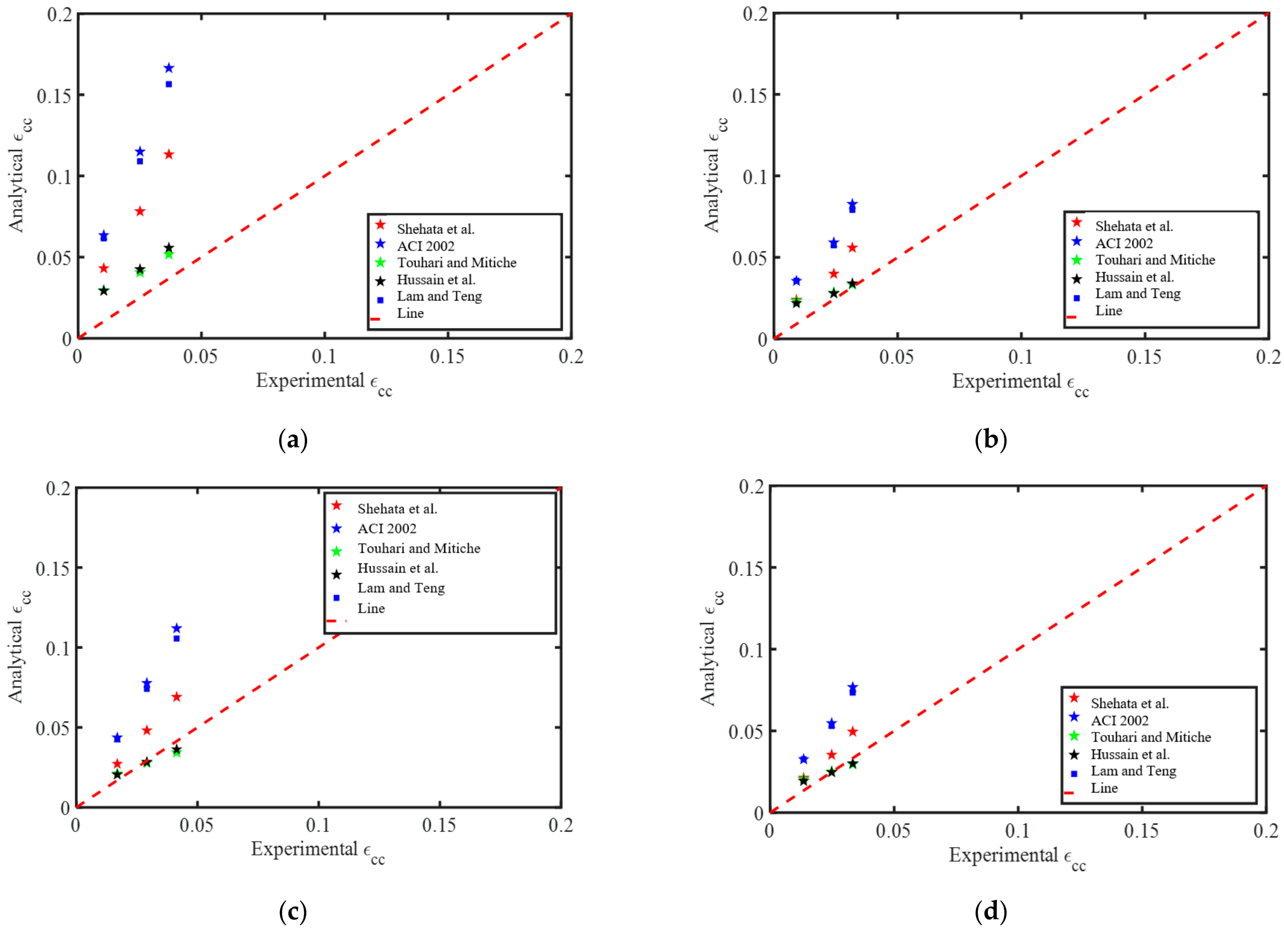

Figure 11. Comparison of experimental and analytical confined ultimate compressive "ϵ_{cc}" for subgroup (**a**) LS-CBA (**b**) HS-CBA (**c**) LS-CBB and (**d**) HS-CBB.

In general, the model of Hussain et al. [39] was able to provide close approximates of experimental peak confined compressive strengths. Table 7 provides summary of the comparison of analytical and experimental ultimate stress-strain values. Accuracy of existing models is assessed by the average of the ratio of analytical to experimental values and associated standard deviations. For ultimate stress predictions, the closest to 1 mean value of the average of analytical to experimental ultimate compressive stress was 0.87 that was provided by the model of Hussain et al. [39]. Same model also yielded lowest standard deviation of analytical to experimental ultimate stress ratios. For ultimate strain predictions, almost all models overestimated experimental ultimate compressive strain values. This overestimation was found prevalent in subgroup LS-CBA. However, none of the considered existing models in this study were able to provide good agreement with experimental ultimate strain values. Therefore, further studies are suggested to enhance the database in terms of axial stress-strain tests of LC-GFRP confined non-circular specimens. With a large sample size, an accurate ultimate stress-strain model can be proposed.

Table 7. Summary of the comparison between experimental and analytically predicted stress-strain values.

ID/Model	$f_{cc,e}$ (MPa)	$\epsilon_{cc,e}$	Shihata et al. [41]		ACI 2002 [28]		Touhari and Mitiche [47]		Hussain et al. [39]		Mirmiran et al. [48]		Lam & Teng [49]	
			$\frac{f_{cc,a}}{f_{cc,e}}$	$\frac{\epsilon_{cc,a}}{\epsilon_{cc,e}}$	$\frac{f_{cc,e}}{f_{cc,a}}$	$\frac{\epsilon_{cc,a}}{\epsilon_{cc,e}}$	$\frac{f_{cc,e}}{f_{cc,a}}$	$\frac{\epsilon_{cc,a}}{\epsilon_{cc,e}}$	$\frac{f_{cc,e}}{f_{cc,a}}$	$\frac{\epsilon_{cc,a}}{\epsilon_{cc,e}}$	$\frac{f_{cc,e}}{f_{cc,a}}$	$\frac{\epsilon_{cc,a}}{\epsilon_{cc,e}}$	$\frac{f_{cc,e}}{f_{cc,a}}$	$\frac{\epsilon_{cc,a}}{\epsilon_{cc,e}}$
LS-CBA-2L	12.9		0.83	4.14	1.53	6.10	0.78	2.83	0.98	2.81	0.81	-	1.35	5.92
LS-CBA-4L	19.5		0.67	3.11	1.31	4.58	0.60	1.62	0.87	1.69	0.61	-	1.35	4.34
LS-CBA-6L	28.3		0.54	3.07	1.02	4.52	0.47	1.40	0.75	1.51	0.46	-	1.25	4.25
HS-CBA-2L	20.9		0.98	2.63	1.55	3.89	0.95	2.55	1.08	2.40	0.97	-	1.30	3.91
HS-CBA-4L	27.1		0.84	1.65	1.54	2.44	0.79	1.17	0.98	1.15	0.80	-	1.34	2.37
HS-CBA-6L	34.2		0.73	1.76	1.42	2.61	0.68	1.05	0.90	1.07	0.67	-	1.32	2.49
LS-CBB-2L	21.3		0.63	1.61	1.11	2.58	0.60	1.25	0.72	1.21	0.62	-	0.94	2.52
LS-CBB-4L	26.4		0.60	1.65	1.16	2.67	0.55	0.95	0.74	0.98	0.55	-	1.10	2.54
LS-CBB-6L	31.8		0.57	1.66	1.11	2.70	0.54	0.83	0.75	0.88	0.49	-	1.20	2.55
HS-CBB-2L	23.6		0.87	1.57	1.37	2.41	0.83	1.52	0.95	1.43	0.86	-	1.15	2.42
HS-CBB-4L	29.9		0.76	1.43	1.39	2.20	0.73	1.01	0.89	0.99	0.72	-	1.21	2.14
HS-CBB-6L	34.8		0.72	1.49	1.40	2.30	0.70	0.89	0.88	0.90	0.65	-	1.30	2.20
Mean =			0.73	2.14	1.33	3.25	0.68	1.42	0.87	1.42	0.68	-	1.23	3.14
Standard Deviation =			0.13	0.88	0.18	1.23	0.14	0.65	0.11	0.61	0.15	-	0.12	1.18

5. Conclusions and Suggestions for Future Research

This study proposed a sustainable and cost-effective solution for the reuse of brick construction waste for structural applications. A total of 32 rectilinear specimens were tested in this in two groups depending upon the constituting brick aggregates types i.e., hollow-clay and solid-clay brick aggregates. Two concrete strengths were considered. Further, to overcome the deficiencies arising from the inherent substandard mechanical properties of brick aggregates in comparison to natural stone aggregates, a cost-effective and environment friendly solution was proposed. Low-cost- GFRP sheets were wrapped around specimens to strengthen their ultimate stress and corresponding strain. Following important conclusions can be drawn.

1. LC-GFRP sheets were able to enhance peak axial stress and corresponding strain of RBAC specimens. This improvement was found to correlate positively with the number of external LC-GFRP layers. For the case of 4 and 6 LC-GFRP layers, a bilinear stress-strain relation was observed exhibiting significant axial ductility.
2. The increase in ultimate stress and strain of RBAC specimens was dependent upon the inherent unconfined concrete strength. For low strength specimens, increase in both ultimate compressive stress and corresponding strain was higher than that observed in high strength concrete specimens.
3. For solid clay brick aggregate concrete, increase in ultimate compressive stress and corresponding strain was found higher than that in hollow-clay brick aggregate concrete. Therefore, it can be established that for same specimen type i.e., concrete strength, size, and mix ratio, specimens constructed with hollow brick aggregates may require higher LC-GFRP amounts to reach similar strength levels as those of solid-clay brick aggregate concrete.
4. Several existing confined axial stress-strain models were assessed to check their accuracy for LC-GFRP confined specimens. It was found that the model of Hussain et al. [39] provided closest approximations of experimental ultimate compressive stresses. Whereas none of the existing models could predict experimental peak strains with good accuracy.
5. The proposed LC-GFRP composites can be widely used to enhance the strength and ductility of reinforced concrete columns, beams, beam-column joints and to replace the existing high-cost carbon fiber reinforced polymer composites.

6. Future studies must be carried to study the influence of steel reinforcement on the strength of the LC-GFRP composites confined reinforced concrete columns and use of brick aggregates on the adhesion of the reinforcing steel to the concrete.

Author Contributions: Conceptualization, K.R. and P.J.; Data curation, Q.H. and P.J.; Supervision, Q.H. and P.J.; Validation, Q.H. and A.W.A.Z.; Writing—original draft, K.R. and Q.H.; Writing—review & editing, N.A. and K.C. All authors have read and agreed to the published version of the manuscript.

Funding: This research was funded by College of Industrial Technology, King Mongkut's University of Technology North Bangkok (Grant No. Res-CIT0288/2022).

Institutional Review Board Statement: Not applicable.

Acknowledgments: This research was funded by College of Industrial Technology, King Mongkut's University of Technology North Bangkok (Grant No. Res-CIT0288/2022). Thanks are also extended to Universiti Kebangsaan Malaysia (UKM) for supporting this research work and Asian Institute of Technology (AIT), Thailand for supporting test facilities.

Conflicts of Interest: The authors declare no conflict of interest.

References

1. Zheng, H.; Yuan-Feng, L. Probe into the Resource Utilization of Abandoned. Google Scholar, Henan Buildings. 2019. Available online: https://scholar.google.com/scholar?hl=en&as_sdt=0%2C5&q=Probe+into+the+resource+utilization+of+abandoned+clay+bricks+in+construction&btnG= (accessed on 28 April 2022).
2. Xiao, J.; Li, W.; Fan, Y.; Huang, X. An overview of study on recycled aggregate concrete in China (1996–2011). *Constr. Build. Mater.* **2012**, *31*, 364–383. [CrossRef]
3. Hamad, B.S.; Dawi, A.H. Sustainable normal and high strength recycled aggregate concretes using crushed tested cylinders as coarse aggregates. *Case Stud. Constr. Mater.* **2017**, *7*, 228–239. [CrossRef]
4. Ohemeng, E.A.; Ekolu, S.O. Comparative analysis on costs and benefits of producing natural and recycled concrete aggregates: A South African case study. *Case Stud. Constr. Mater.* **2020**, *13*, e00450. [CrossRef]
5. Hussain, I.; Ali, B.; Akhtar, T.; Jameel, M.S.; Raza, S.S. Comparison of mechanical properties of concrete and design thickness of pavement with different types of fiber-reinforcements (steel, glass, and polypropylene). *Case Stud. Constr. Mater.* **2020**, *13*, e00429. [CrossRef]
6. Poon, C.S.; Kou, S.C.; Lam, L. Use of recycled aggregates in molded concrete bricks and blocks. *Constr. Build. Mater.* **2002**, *16*, 281–289. [CrossRef]
7. Sagoe-Crentsil, K.; Brown, T.; Taylor, A. Performance of concrete made with commercially produced coarse recycled concrete aggregate. *Cem. Concr. Res.* **2001**, *31*, 707–712. [CrossRef]
8. RILEM—Specifications for Concrete with Recycled Aggregates. *Mater. Struct.* **1994**, *27*, 557–559. Available online: https://www.rilem.net/publication/publication/279?id_papier=6137 (accessed on 28 April 2022). [CrossRef]
9. Manfredi, S.; Pant, R.; Pennington, D.W.; Versmann, A. Supporting environmentally sound decisions for waste man-agement with LCT and LCA. *Int. J. Life Cycle Assess.* **2011**, *16*, 937–939. [CrossRef]
10. Chaiyasarn, K.; Hussain, Q.; Joyklad, P.; Rodsin, K. New hybrid basalt/E-glass FRP jacketing for enhanced confinement of recycled aggregate concrete with clay brick aggregate. *Case Stud. Constr. Mater.* **2021**, *14*, e00507. [CrossRef]
11. Ge, Z.; Wang, Y.; Sun, R.; Wu, X.; Guan, Y. Influence of ground waste clay brick on properties of fresh and hardened concrete. *Constr. Build. Mater.* **2015**, *98*, 128–136. [CrossRef]
12. Zhao, C.; Zheng, C.; Zhao, M.; Tu, Y.; Liu, J. Multivariate autoregressive models and kernel learning algorithms for classifying driving mental fatigue based on electroencephalographic. *Expert Syst. Appl.* **2011**, *38*, 1859–1865. [CrossRef]
13. Gao, C.; Huang, L.; Yan, L.; Jin, R.; Chen, H. Mechanical properties of recycled aggregate concrete modified by nano-particles. *Constr. Build. Mater.* **2020**, *241*, 118030. [CrossRef]
14. Khalaf, F.M. Using Crushed Clay Brick as Coarse Aggregate in Concrete. *J. Mater. Civ. Eng.* **2006**, *18*, 518–526. [CrossRef]
15. Khalaf, F.M.; DeVenny, A.S. Performance of Brick Aggregate Concrete at High Temperatures. *J. Mater. Civ. Eng.* **2004**, *16*, 556–565. [CrossRef]
16. Hansen, T.C. Recycling of Demolished Concrete and Masonry: Report of Technical Committee 37-DRC, Demolition and Reuse of Concrete, E & FN Spon. 1992. Available online: https://www.routledge.com/Recycling-of-Demolished-Concrete-and-Masonry/Hansen/p/book/9780419158202 (accessed on 28 April 2022).
17. Khalaf, F.M.; Devenny, A.S. Recycling of Demolished Masonry Rubble as Coarse Aggregate in Concrete: Review. *J. Mater. Civ. Eng.* **2004**, *16*, 331–340. [CrossRef]
18. Akhtaruzzaman, A.A.; Hasnat, A. Properties of Concrete Using Crushed Brick as Aggregate. *Concr. Int.* **1983**, *5*, 58–63.
19. Debieb, F.; Kenai, S. The use of coarse and fine crushed bricks as aggregate in concrete. *Constr. Build. Mater.* **2008**, *22*, 886–893. [CrossRef]

20. Yang, Y.-F.; Ma, G.-L. Experimental behaviour of recycled aggregate concrete filled stainless steel tube stub columns and beams. *Thin-Wall. Struct.* **2013**, *66*, 62–75. [CrossRef]
21. Adamson, M.; Razmjoo, A.; Poursaee, A. Durability of concrete incorporating crushed brick as coarse aggregate. *Constr. Build. Mater.* **2015**, *94*, 426–432. [CrossRef]
22. Vrijders, J.; Desmyter, J. Een Hoogwaardig Gebruik van Puingranulaten Stimuleren, OVAM Mechelen. 2008. Available online: https://www.ovam.be/sites/default/files/FILE1297949793382080915_Hoogwaardig_gebruik_puingranulaten.pdf (accessed on 22 April 2022).
23. Poon, C.S.; Chan, D. Feasible use of recycled concrete aggregates and crushed clay brick as unbound road sub-base. *Constr. Build. Mater.* **2006**, *20*, 578–585. [CrossRef]
24. Gao, C.; Huang, L.; Yan, L.; Kasal, B.; Li, W. Behavior of glass and carbon FRP tube encased recycled aggregate concrete with recycled clay brick aggregate. *Compos. Struct.* **2016**, *155*, 245–254. [CrossRef]
25. Tang, Z.; Li, W.; Tam, V.W.; Yan, L. Mechanical performance of CFRP-confined sustainable geopolymeric recycled concrete under axial compression. *Eng. Struct.* **2020**, *224*, 111246. [CrossRef]
26. Hassan, S.H.; Rasheed, L.S.; Salih, S.A. The repair of recycled crushed brick aggregate RC beams with shear deficiencies with CFRP. *IOP Conf. Ser. Mater. Sci. Eng.* **2021**, *1067*, 012048. [CrossRef]
27. Chen, G.M.; Zhang, J.J.; Jiang, T.; Lin, C.J.; He, Y.H. Compressive Behavior of CFRP-Confined Recycled Aggregate Concrete in Different-Sized Circular Sections. *J. Compos. Constr.* **2018**, *22*, 04018021. [CrossRef]
28. Islam, M.; Choudhury, M.S.I.; Amin, A.F.M.S. Dilation Effects in FRP-Confined Square Concrete Columns Using Stone, Brick, and Recycled Coarse Aggregates. *J. Compos. Constr.* **2015**, *20*, 04015017. [CrossRef]
29. Yooprasertchai, E.; Dithaem, R.; Arnamwong, T.; Sahamitmongkol, R.; Jadekittichoke, J.; Joyklad, P.; Hussain, Q. Remediation of punching shear failure using glass fiber reinforced polymer (GFRP) rods. *Polymers* **2021**, *13*, 2369. [CrossRef] [PubMed]
30. Iskander, M.; Hassan, M. State of the Practice Review in FRP Composite Piling. *J. Compos. Constr.* **1998**, *2*, 116–120. [CrossRef]
31. Yoddumrong, P.; Rodsin, K.; Katawaethwarag, S. Seismic strengthening of low-strength RC concrete columns using low-cost glass fiber reinforced polymers (GFRPs). *Case Stud. Constr. Mater.* **2020**, *13*, e00383. [CrossRef]
32. Rodsin, K.; Hussain, Q.; Suparp, S.; Nawaz, A. Compressive behavior of extremely low strength concrete confined with low-cost glass FRP composites. *Case Stud. Constr. Mater.* **2020**, *13*, e00452. [CrossRef]
33. *ASTM C1314-21*; Standard Test Method for Compressive Strength of Masonry Prisms. ASTM International: West Conshohocken, PA, USA, 2021.
34. *ASTM C140/C140M-22a*; Standard Test Methods for Sampling and Testing Concrete Masonry Units and Related Units. 2022. Available online: https://www.astm.org/c0140-c0140m-22a.html (accessed on 23 April 2022).
35. *ASTM D3013-13*; Standard Specification for Epoxy Molding Compounds. 2021. Available online: https://www.astm.org/d3013-13.html (accessed on 30 April 2022).
36. Mostofinejad, D.; Moshiri, N.; Mortazavi, N. Effect of corner radius and aspect ratio on compressive behavior of rec-tangular concrete columns confined with CFRP. *Mater. Struct. Mater. Construct.* **2015**, *48*, 107–122. [CrossRef]
37. Wang, L.-M.; Wu, Y.-F. Effect of corner radius on the performance of CFRP-confined square concrete columns: Test. *Eng. Struct.* **2008**, *30*, 493–505. [CrossRef]
38. Soudki, K.; Alkhrdaji, T. Guide for the Design and Construction of Externally Bonded FRP Systems for Strengthening Concrete Structures (ACI 440.2R-02). In *Structures Congress and Exposition*; ASCE: Reston, VA, USA, 2005; pp. 1–8. [CrossRef]
39. Hussain, Q.; Ruangrassamee, A.; Tangtermsirikul, S.; Joyklad, P.; Wijeyewickrema, A.C. Low-Cost Fiber Rope Reinforced Polymer (FRRP) Confinement of Square Columns with Different Corner Radii. *Buildings* **2021**, *11*, 355. [CrossRef]
40. Saleem, S.; Hussain, Q.; Pimanmas, A. Compressive Behavior of PET FRP–Confined Circular, Square, and Rectangular Concrete Columns. *J. Compos. Constr.* **2016**, *21*, 04016097. [CrossRef]
41. Shehata, I.A.E.M.; Carneiro, L.; Shehata, L.C.D. Strength of short concrete columns confined with CFRP sheets. *Mater. Struct.* **2002**, *35*, 50–58. [CrossRef]
42. Pimanmas, A.; Hussain, Q.; Panyasirikhunawut, A.; Rattanapitikon, W. Axial strength and deformability of concrete confined with natural fibre-reinforced polymers. *Mag. Concr. Res.* **2018**, *71*, 55–70. [CrossRef]
43. Richart, F.E.; Brandtzæg, A.; Brown, R.L. A Study of the Failure of Concrete under Combined Compressive Stresses, Bulletins—Engineering Experiment Station. 1928. Available online: http://hdl.handle.net/2142/4277 (accessed on 6 March 2022).
44. Miyauchi, K. Estimation of Strengthening Effects with Crbon Feber Sheet for Concrete Column. In Proceedings of the 3rd International Symposium on Non-Metallic (FRP) Reinforcement for Concrete Structures, Sapporo, Japan, 14–16 October 1997; Japan Concrete Institute: Tokyo, Japan, 1997; pp. 217–224. Available online: https://ci.nii.ac.jp/naid/80009963999/ (accessed on 6 March 2022).
45. Benzaid, R.; Mesbah, H.; Chikh, N.E. FRP-confined Concrete Cylinders: Axial Compression Experiments and Strength Model. *J. Reinf. Plast. Compos.* **2010**, *29*, 2469–2488. [CrossRef]
46. Behavior of RC Deep Beams Strengthened in Shear using Glass Fiber Reinforced Polymer with Mechanical Anchors. In Proceedings of the International Conference on Environment and Civil Engineering (ICEACE'2015), Pattaya, Thailand, 24–25 April 2015. [CrossRef]
47. Touhari, M.; Mitiche, R.K. Strength model of FRP confined concrete columns based on analytical analysis and exper-imental test. *Int. J. Struct. Integr.* **2020**, *11*, 82–106. [CrossRef]

48. Mirmiran, A.; Shahawy, M.; Samaan, M.; El Echary, H.; Mastrapa, J.C.; Pico, O. Effect of Column Parameters on FRP-Confined Concrete. *J. Compos. Constr.* **1998**, *2*, 175–185. [CrossRef]
49. Lam, L.; Teng, J.G. Strength Models for Fiber-Reinforced Plastic-Confined Concrete. *J. Struct. Eng.* **2002**, *128*, 612–623. [CrossRef]